J. Fluid Mech. (1982), *vol.* 114, *pp.* 261–282
Printed in Great Britain

Thermal cellular convection in rotating rectangular boxes

By K. BÜHLER AND H. OERTEL
Institut für Strömungslehre und Strömungsmaschinen,
Universität (TH) Karlsruhe, Germany

(Received 28 October 1980 and in revised form 12 May 1981)

The thermal cellular convection in rotating rectangular boxes has been investigated both theoretically and experimentally. In the theoretical analysis, a linear stability theory is used to calculate the stability behaviour and the configuration of the three-dimensional convection flow. The numerical results show that the rolls change their orientation for a Taylor number greater than a critical value. In the experimental investigation, the flow patterns were visualized by a special differential interferometer. The experimental results are presented in stability diagrams and interferogram series which demonstrate the influence of rotation as well as initial and boundary conditions on the convective flow. We found that the effects of the Coriolis force and those of centrifugal forces could be studied separately by the choice of different test fluids, e.g. nitrogen is good for the Coriolis-force effect while silicone oil is good for the centrifugal-force effect.

When compared with experimental results, our theoretical model is shown to be good for fluids of small Prandtl number such as nitrogen gas. We also compare our results with the well-known asymptotic behaviour of the critical Rayleigh number and wavenumber.

1. Introduction

Thermal instabilities in horizontal fluid layers are of both practical and theoretical interest. In the fields of crystal growth, geophysics and meteorology, the physical boundaries and the superimposed rotational motion play an essential role. In the books of Chandrasekhar (1961) and Gershuni & Zukhovitskii (1976) and in the papers of Ostrach (1972), Oertel (1979, 1980) and Hopfinger, Atten & Busse (1979), the theoretical and experimental results are comprehensively presented.

The onset of cellular convection in rectangular containers was treated theoretically by Davis (1967) and Catton (1970) and experimentally by Stork & Müller (1972). The influence of rotation on horizontal fluid layers was studied experimentally by Koschmieder (1967) and Rossby (1969).

Theoretical results of the influence of convection in rotating fluid layers were determined by Chandrasekhar (1961), Veronis (1968) and Hunter & Riahi (1975). Sommerville & Lipps (1973) calculated three-dimensional cell structure. The stability behaviour was treated by Küppers & Lortz (1969), Küppers (1970) and Clever & Busse (1979). The influence of vertical boundaries on cellular convection in rotating systems has been investigated theoretically by Davies-Jones & Gilman (1971) and Gilman (1973) for a circular annulus. Homsy & Hudson (1972) calculated the stability behaviour in a cylindrical container. The influence of the centrifugal force

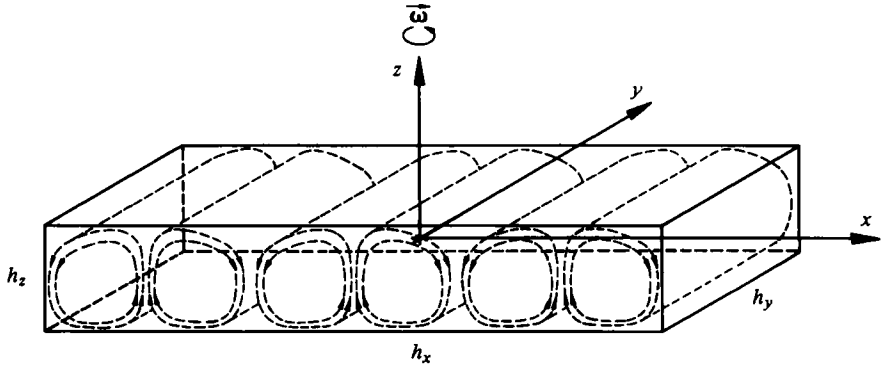

FIGURE 1. Rectangular annulus geometry with rotation axis.

has been investigated both theoretically and experimentally by Torrest & Hudson (1974), Abell & Hudson (1975) and Hudson (1970). Homsy & Hudson (1971*b*) showed, with an asymptotic theory, that the centrifugal circulation stabilizes the layer everywhere except near vertical boundaries, where it is slightly destabilizing.

The known results from the literature are that rotational effects have in some cases a strong influence on convection flows. The following questions are treated in this paper.

(i) What influence have the rotation and side boundaries (box geometry) on the convective stability and flow configuration?

(ii) In which region can the following physical model with the Boussinesq approximation be applied?

(iii) What behaviour have the asymptotic solutions for convection in boxes?

We applied interferometric measuring techniques for the visualization and quantitative interpretation of convection flow in the investigation of cellular convection in a rotating system. The application of optical measuring techniques makes the use of rectangular containers necessary. Rectangular boxes have another advantage in that the convection rolls are oriented along the shorter side of the container, thereby minimizing the viscous drag. The influence of the Coriolis and centrifugal forces can therefore be investigated systematically.

2. Theory

2.1. *Basic equations*

The conservation equations for mass, momentum and energy are expressed in Boussinesq form. A linear relation between density and temperature is used. Extensive descriptions of the Boussinesq approximation are given by Spiegel & Veronis (1960) and Gray & Giorgini (1976). Figure 1 shows the rectangular box with the Cartesian co-ordinate system and the vertical rotation axis. The dimensionless variables are found by using h_z, h_z^2/κ, $T_1 - T_2$, $\rho\nu\kappa/h_z^2$ as the scales for length, time, temperature and pressure. The dimensionless linearized perturbation equations are

$$\nabla . \mathbf{v} = 0, \tag{2.1}$$

$$\Delta \mathbf{v} + RaT^* \mathbf{e}_z - Ta^{\frac{1}{2}}(\mathbf{e}_z \times \mathbf{v}) - \nabla p^* = 0, \tag{2.2}$$

$$\Delta T^* + w = 0, \tag{2.3}$$

with the two non-dimensional parameters, the Rayleigh number Ra and the Taylor number Ta, given by

$$Ra = \frac{g\alpha h_z^3(T_1 - T_2)}{\nu\kappa}, \quad Ta = \frac{4\omega^2 h_z^4}{\nu^2}. \tag{2.4}$$

In the above κ is the thermal diffusivity, ν the kinematic viscosity, α the thermal expansion coefficient, h_z the height of the convection box, T_1 and T_2 the temperatures at the lower and upper horizontal plates respectively, ω the angular velocity and $\mathbf{e}_z$ the unit vector in the vertical direction; T^* and p^* are the perturbation temperature and pressure and $\mathbf{v}$ the relative velocity, which together describe the deviation from the basic heat conduction state.

In this physical model, we have neglected centrifugal effects as a consequence of the Boussinesq approximation. Essentially we accept the argument given by Greenspan (1968), that is, we assume centrifugal acceleration is very small compared with gravity, which requires

$$\omega^2 r/g \ll 1, \tag{2.5}$$

where r is a mean radius. Then temperature and density in the basic state are functions of height only and the centrifugally induced circulation is very small and negligible compared with the convective instabilities.

The horizontal and vertical boundaries of the rectangular box are assumed to be rigid and perfectly conducting. The boundary conditions are

$$\left.\begin{aligned} \mathbf{v} &= 0 \\ T^* &= 0 \end{aligned}\right\} \quad \text{for} \quad x = \pm\tfrac{1}{2}H_x, \quad y = \pm\tfrac{1}{2}H_y, \quad z = \pm\tfrac{1}{2}, \tag{2.6}$$

in which $H_x = h_x/h_z$ and $H_y = h_y/h_z$ are the dimensionless length and depth of the box.

2.2. *Galerkin method*

A Galerkin method has been used to solve the linear Boussinesq equations (2.1)–(2.3) with the boundary conditions (2.6). For convection flow the application is described by Finlayson (1968) and Gershuni & Zukhovitskii (1976). The velocity field of cellular convection in rotating rectangular boxes is three-dimensional. We also assume that the velocity field should be divergence free. The continuity equation is thereby exactly satisfied and the pressure can be eliminated from the equations through the stream-function formulation. The velocity field is chosen so that the properties of the differential equations and the boundary conditions are satisfied. The three-dimensional velocity field is found by superposition of two planar motions in the following form as described by Davis (1967) and Catton (1970):

$$\mathbf{v} = \sum_{j=1}^{N} a_j \mathbf{v}_j(x, y, z), \quad \mathbf{v}_j = \mathbf{v}_{1j} + \mathbf{v}_{2j} = \operatorname{curl}(\mathbf{e}_y \psi_j) + \operatorname{curl}(\mathbf{e}_x \phi_j), \tag{2.7}$$

$$T^* = \sum_{j=1}^{N} b_j T_j^*(x, y, z), \quad T_j^* = T_{1j}^* + T_{2j}^*, \tag{2.8}$$

$$\left.\begin{aligned} \mathbf{v}_{1j} &= 0 \\ T_{1j}^* &= 0 \end{aligned}\right\} \quad \text{for} \quad j > \tfrac{1}{2}N, \qquad \left.\begin{aligned} \mathbf{v}_{2j} &= 0 \\ T_{2j}^* &= 0 \end{aligned}\right\} \quad \text{for} \quad j < \tfrac{1}{2}N;$$

ψ_j and ϕ_j are stream functions in the (x, z)- and (y, z)-planes. This approximation was compared by Frick & Clever (1980) with a general three-dimensional representation

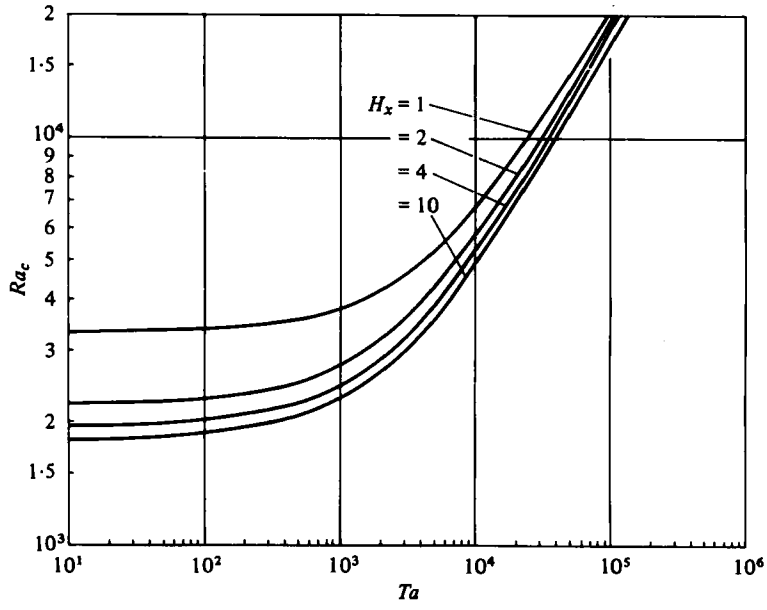

FIGURE 2. Critical Rayleigh number as a function of the Taylor number. H_x and H_y are dimensionless lengths in the x- and y-directions. $H_y = 4$.

	Box $H_x = 10$, $H_y = 4$		Infinite layer	
Ta	Ra_c	a_c	Ra_c	a_c
0	1815·2	3·14	1707·8	3·117
10^2	1861·6	3·14	1756·6	3·15
10^3	2277·4	3·46	2151·7	3·50
10^4	4918·0	5·50	4713·1	4·80
10^5	17268·8	7·07	16721·0	7·20

TABLE 1. Critical Rayleigh and wavenumbers, box $H_x = 10$, $H_y = 4$ compared with the infinite layer from Chandrasekhar (1961).

of the toroidal and poloidal vector field in the case of both free and rigid upper and lower boundaries with rigid side walls. They found that the critical Rayleigh number of the approximation used here does not differ substantially from the general three-dimensional results, especially for our aspect ratio. The functions for the perturbation temperature are assumed to be scalar, so that they are directly proportional to the vertical velocity. In the calculations, the number of trial functions N used is always 112.

The orthogonality relation requires the following Galerkin equations:

$$\sum_{j=1}^{N} (a_j[\int \mathbf{v}_k \Delta \mathbf{v}_j dV - Ta^{\frac{1}{2}} \int (\mathbf{e}_z \times \mathbf{v}_j)\, \mathbf{v}_k\, dV] + b_j Ra \mathbf{e}_z \int \mathbf{v}_k T_j^*\, dV) = 0, \tag{2.9}$$

$$\sum_{j=1}^{N} (a_j \mathbf{e}_z \int \mathbf{v}_j T_k^*\, dV + b_j \int T_k^* \Delta T_j^*\, dV) = 0, \quad k = 1, 2, \ldots, N. \tag{2.10}$$

The equations (2.9) and (2.10) represent a linear homogeneous system of algebraic equations for the $2N$ unknown coefficients a_j and b_j. For a given Taylor number and

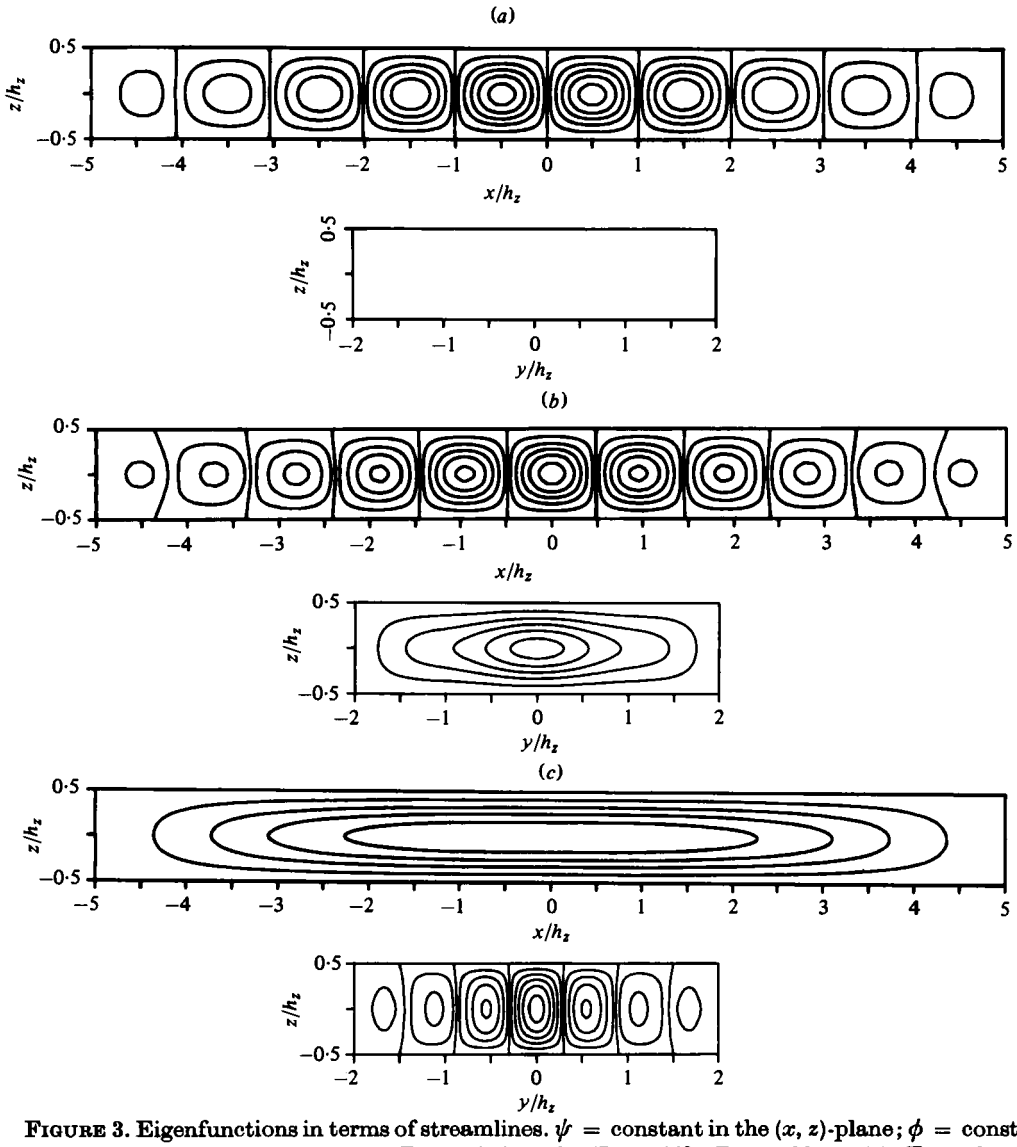

FIGURE 3. Eigenfunctions in terms of streamlines. ψ = constant in the (x, z)-plane; ϕ = constant in the (y, z)-plane. (*a*) $Ta = 0$, $Ra_c = 1815$; (*b*) $Ta = 10^3$, $Ra_c = 2277$; (*c*) $Ta = 2 \times 10^4$, $Ra_c = 6855$.

for certain Rayleigh numbers only this system has a non-trivial solution. The smallest eigenvalue is the critical Rayleigh number. The formulation of the trial functions and the reduced eigenvalue problem are described in the appendix.

2.3. *Numerical results*

(*a*) *Onset of cellular convection.* The stability behaviour of this linear theory refers to the onset of cellular convection when the periodic convection superimposes itself on the steady heat conduction state. In figure 2 the critical Rayleigh numbers are plotted as functions of the Taylor number. The individual curves are distinguished by the geometry of the rectangular box. The ordinate with $Ta \to 0$ gives the limiting case

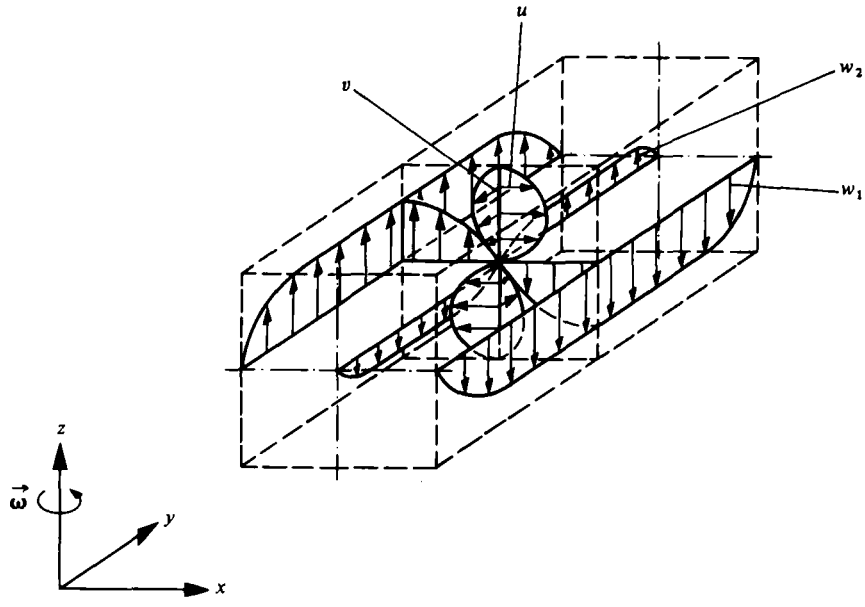

FIGURE 4. Velocity distribution in a convection roll. $\mathbf{v}_1 = (u, 0, w_1)$ flow in the (x, z)-plane; $\mathbf{v}_2 = (0, v, w_2)$ flow in the (y, z)-plane.

without rotation. The critical Rayleigh number increases as the size of the box decreases. The influence of the side walls has a stabilizing effect because of the additional viscous shear. The onset of convection occurs at larger critical Rayleigh numbers. With the superposition of rotation which is characterized by the Taylor number, the critical Rayleigh number increases further. This effect results from the action of the Coriolis force perpendicular to the direction of the relative velocity, which dampens the onset of convective instabilities. However, with increasing Taylor number the box geometry has a lessening influence on the critical Rayleigh number. Therefore, the stability curves converge for large Taylor numbers. With increasing Taylor number the influence of the Coriolis force increasingly dominates that of the side walls. In table 1 the critical Rayleigh numbers for the box with $H_x = 10$, $H_y = 4$ which is investigated in the experiments, is compared with the critical Rayleigh numbers for horizontal layers without side walls.

For Taylor numbers $Ta > 10^5$ the stability curves change into the asymptotic solution, whose gradient is proportional to $\frac{2}{3}$ the power of the Taylor number. For the limiting case $Ta \to \infty$ the convection flow is suppressed, provided the Rayleigh number Ra is finite and fixed.

(*b*) *Convective flow structure.* The eigenfunctions describe the solutions for the velocity and temperature fields which have been determined from the eigenvalue problem with the exception of one constant. From both of the partial solutions, which yield by superposition the three-dimensional velocity field, the stream functions are plotted in figure 3. The convection movement resulting from the stream function ψ in the (x, z)-plane for $Ta = 0$ is graphed in figure 3 (*a*). In the (y, z)-plane no movements exist. The convection movement has the two velocity components u and w_1, which are dependent on all three co-ordinates. With increasing Taylor number the influence of

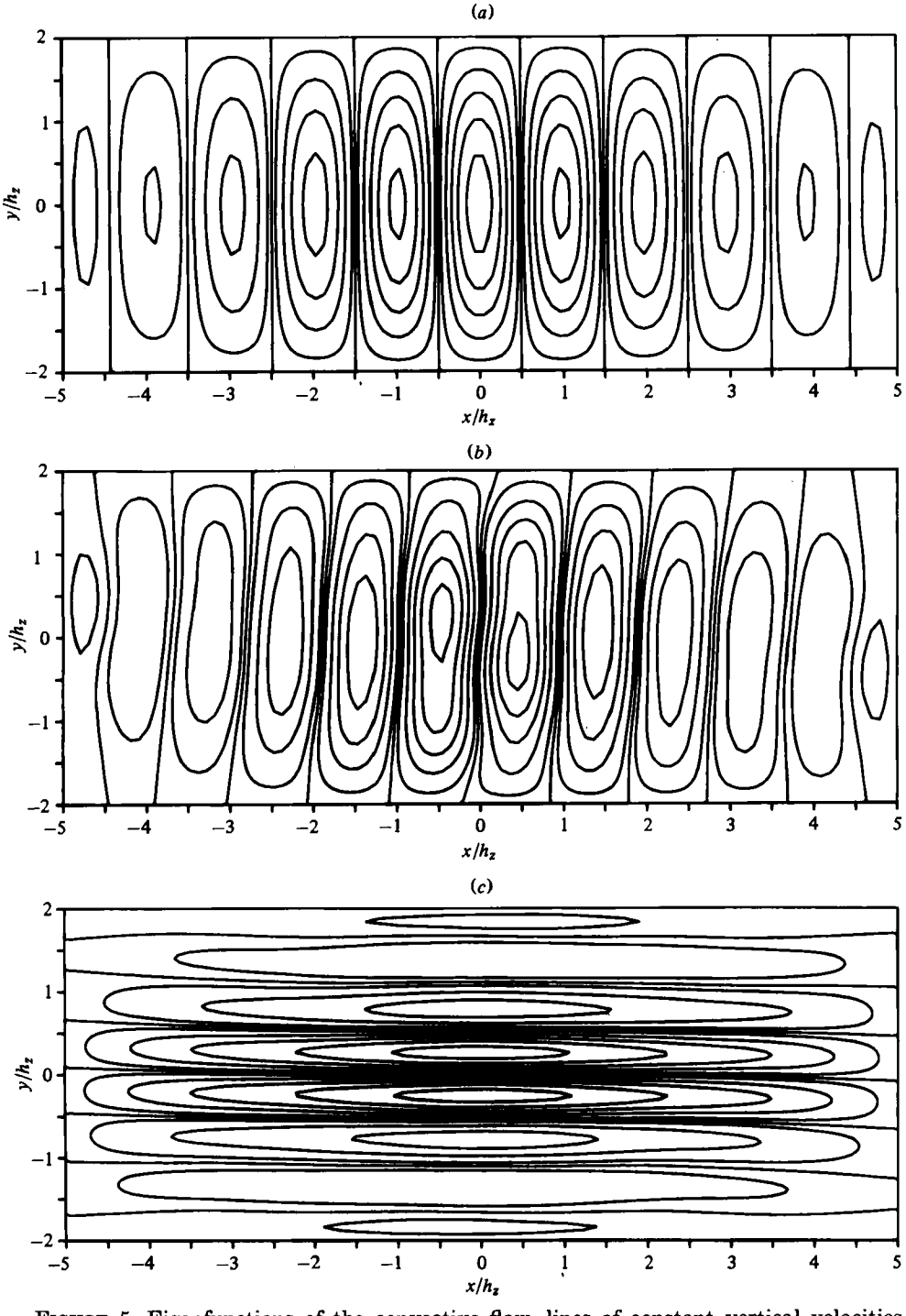

FIGURE 5. Eigenfunctions of the convective flow, lines of constant vertical velocities in the (x, y)-plane. (*a*) $Ra_c = 1815$, $Ta = 0$; (*b*) $Ra_c = 2277$, $Ta = 10^3$; (*c*) $Ra_c = 6855$, $Ta = 2 \times 10^4$.

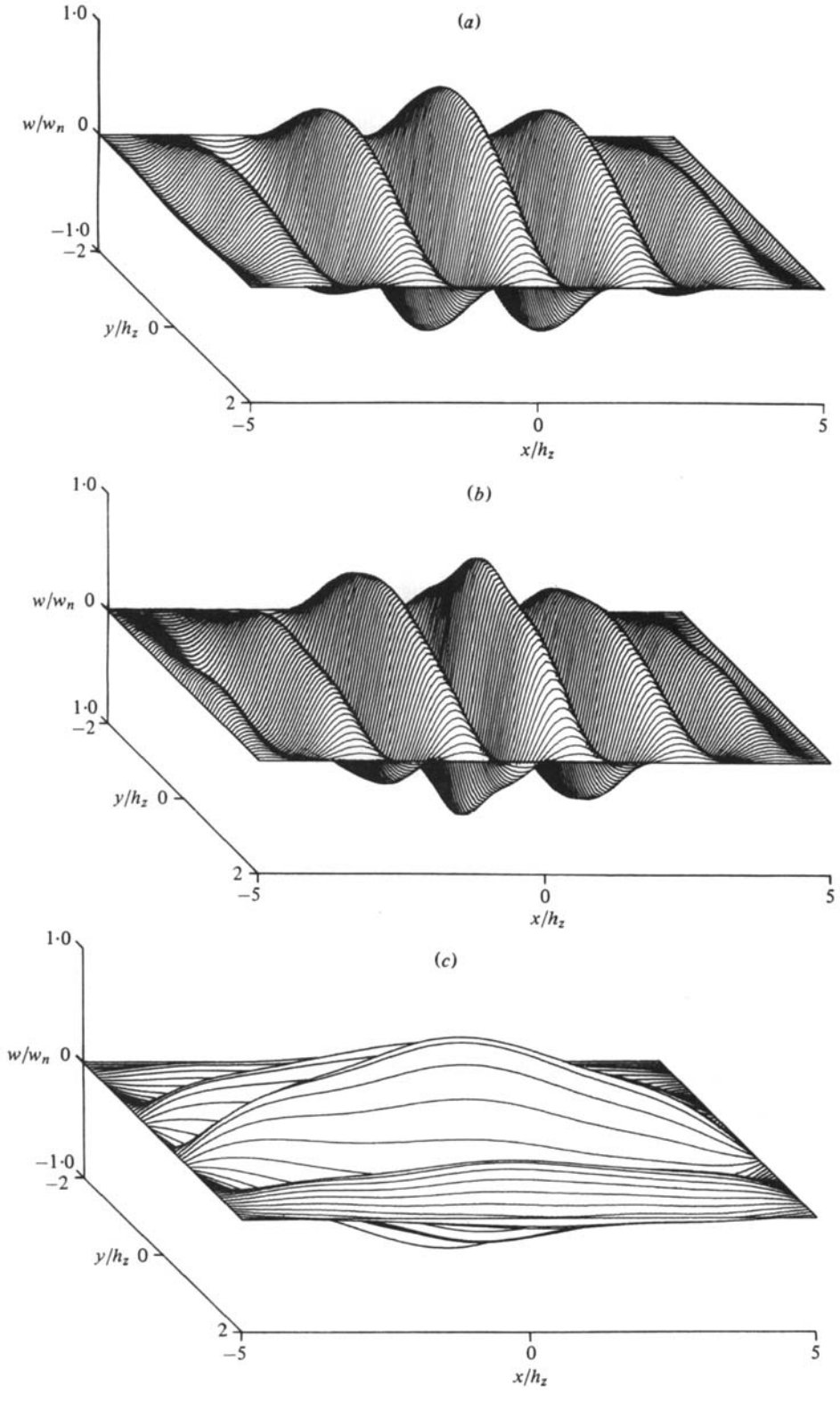

FIGURE 6. Amplitude of the three-dimensional vertical velocities normalized with w_n. (a) $Ra_c = 1815$, $Ta = 0$; (b) $Ra_c = 2277$, $Ta = 10^3$; (c) $Ra_c = 6855$, $Ta = 2 \times 10^4$.

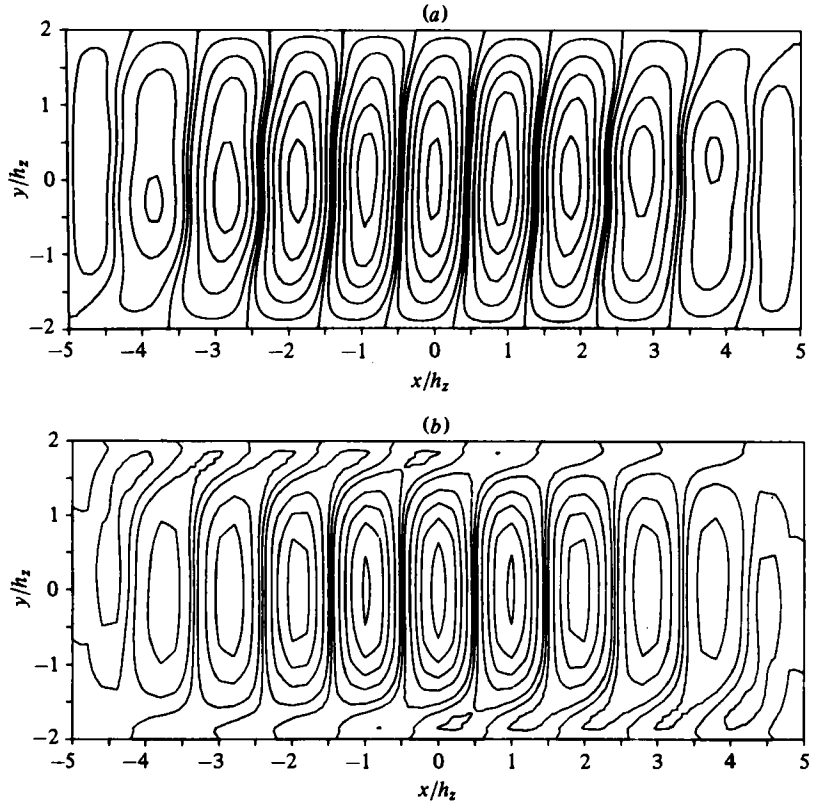

FIGURE 7. Comparison of theoretical results, box $H_x = 10$, $H_y = 4$. The structure of $w(x, y)$, $Ra_c = 2341$, $Ta = 10^3$. (*a*) Galerkin method, linear theory; (*b*) finite-difference method, non-linear theory, $Pr = 0{\cdot}7$.

the Coriolis force in the (y, z)-plane becomes visible as shown in figure 3(*b*). This movement has the velocity components v and w_2 resulting from the stream function ϕ in the (y, z)-plane. The superposition of the flow in the (x, z)-plane and (y, z)-plane gives the three-dimensional flow field as shown in figure 4.

The velocity component v is linked to the u velocity component because of the Coriolis force. For a Taylor number $Ta > 1500$ in the box with $H_x = 10$ and $H_y = 4$ the velocity component v becomes bigger than u and movement in the (y, z)-plane is preferred by the periodic motion. The flow then develops as shown in figure 3(*c*) for $Ta = 2 \times 10^4$.

Figure 3 shows the decreasing wavelength with increasing Taylor number. The dimensionless wavenumber as function of the Taylor number is graphed in figure 15 with the experimental results. The asymptotic solution of the dimensionless wavenumber which is proportional to the $\frac{1}{6}$ power of the Taylor number can be predicted using the linear stability theory. Lines of constant vertical velocities are plotted in figure 5. The dimensionless velocity is normalized to the value 1. In figure 5(*a*) the convection movement is graphed in the (x, y)-plane for $Ta = 0$. The 10 convection rolls in the box of length $H_x = 10$ are oriented parallel to the shorter side. With increasing Taylor number the influence of the Coriolis force becomes visible. The movement in the (y, z)-plane is induced by the Coriolis acceleration. Eleven convection

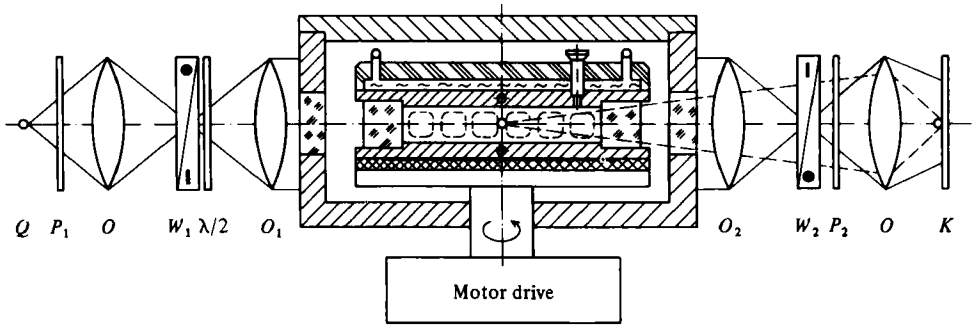

FIGURE 8. Experimental set-up: differential interferometer and convection box.

rolls can be seen at the Taylor number $Ta = 10^3$ in figure 5(*b*). The rolls are oriented parallel to the longer side of the rectangular box with $H_x = 10$, $H_y = 4$ for $Ta > 1500$. The flow then develops as shown in figure 5(*c*) for $Ta = 2 \times 10^4$. The Taylor number at which this cell orientation changes, increases as the size of the rectangular box decreases. These cell structure changes were discussed by Gilman (1973), but with his special eigenfunctions it was not possible to show this effect.

The three-dimensional eigenfunctions are plotted in figure 6 for three different Taylor numbers. The vertical velocity distribution in the (x, y)-plane is shown in the box with $H_x = 10$, $H_y = 4$. The flow structure is graphed in figure 6(*a*) for the non-rotating case. In the direction of the roll axis the vertical velocity increases monotonically from the boundary to the middle of the box. At the Taylor number $Ta = 10^3$, as shown in figure 6(*b*), the amplitude of this velocity component is modulated by the influence of the Coriolis force. The cell structure changes with increasing Taylor number because of the Coriolis force as shown in figure 6(*c*) for $Ta = 2 \times 10^4$.

The theoretical model with the assumptions of the Boussinesq approximation and the restriction to the Coriolis force was proved by Oertel (1981) with a finite-difference method. The comparison of the flow structure resulting from both methods is shown in figure 7. The validity of the linear theory is restricted to the region near the critical state.

3. Experiments

3.1. *Facility*

The experimental set-up is shown in figure 8. The differential interferometer is fixed on an optical bench. The test chamber is set on a rotating table. The convection box rotates inside a vacuum chamber insulating the thermal disturbances from the surroundings. A motor triggered camera registers the interferograms. The exposure time was chosen to be much smaller than the rotation time of the container. The experiments have been done up to a rotation rate of 150 rev./min. The test chamber consists of a rectangular convection box of length $H_x = 10$ and depth $H_y = 4$ with horizontal copper and vertical quartz glass plates. The lower horizontal surface is electrically heated and the upper one has a thermostat-controlled constant temperature. The temperatures were measured using thermistors.

$\rho(T) = 989(1-0{\cdot}00096T)$ (kg m^{-3})
$\nu(T) = 294{\cdot}81\times10^{-6}\exp(-2{\cdot}0934\times10^{-2}T)$ (m^2 s^{-1})
$\alpha = 9{\cdot}6\times10^{-4}$ (K^{-1})
$\lambda = 0{\cdot}1591$ (W m^{-1} K^{-1})
$c = 1507{\cdot}25$ (J kg^{-1} K^{-1})

(*a*) Silicone oil, M200, p = 1013 mbar, T in (°C)

T	10	20	30	40	(°C)
$\rho(T)$	1·2061	1·1649	1·1263	1·0903	(kg m^{-3})
$\nu(T)$	1·4170	1·5058	1·5976	1·6923	$\times10^{-5}$ (m^2 s^{-1})
$\alpha(T)$	3·543	3·419	3·308	3·201	$\times10^{-3}$ (K^{-1})
$\lambda(T)$	0·0248	0·0255	0·0264	0·0271	(W m^{-1} K^{-1})
$c_p(T)$	1041·17	1041·17	1041·20	1041·30	(J kg^{-1} K^{-1})

(*b*) Nitrogen, p = 1013 mbar

TABLE 2. Test fluid properties.

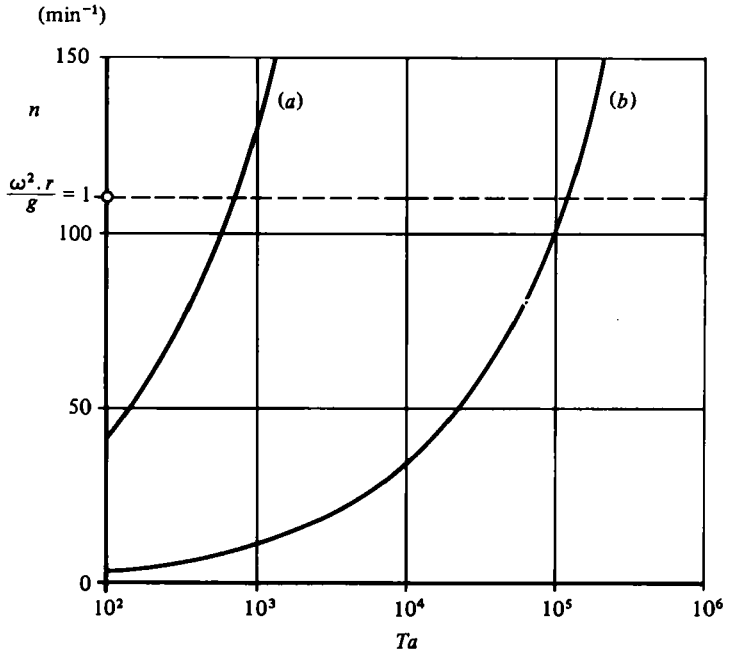

FIGURE 9. Taylor number as a function of the rotation speed for the test fluids (*a*) silicone oil and (*b*) nitrogen.

3.2. *Test fluids*

The test fluids used were silicone oil M200 with a Prandtl number Pr = 1780 and nitrogen with Pr = 0·7. The test fluid properties are tabulated as functions of the temperature in table 2. The corresponding Taylor numbers are graphed in figure 9. For the same speed of revolution the Taylor number in nitrogen is larger than that in silicone oil by a factor of 10^2. Owing to this the influence of the Coriolis and centrifugal forces can be studied approximately independently of each other. The square root of the Taylor number characterizes the influence of the Coriolis force in comparison with

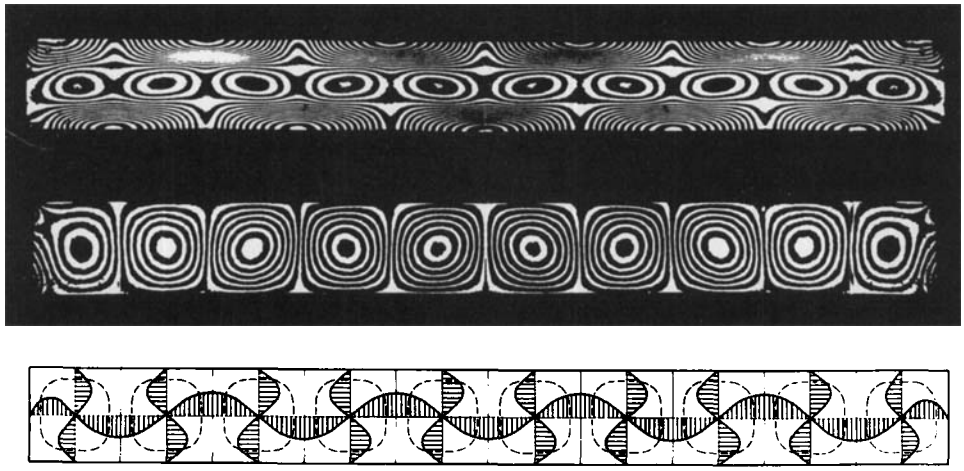

FIGURE 10. Steady convection in silicone oil without rotation, box $H_x = 10$, $H_y = 4$. (*a*) Lines of equal vertical density differences, $Ra = 6270$. (*b*) Lines of equal horizontal density differences, $Ra = 1912$. (*c*) Principal sketch of the velocity distribution.

the friction forces. The Taylor number and therefore the influence of the Coriolis force can be increased by choosing media with less viscosity. In gases the influence of the Coriolis force dominates that of the centrifugal force. In gases, therefore, the theoretical assumptions are especially well satisfied.

3.3. *Measuring technique*

Differential interferometry was used to visualize the convective flow and to evaluate quantitatively the density profiles. The method is described by Oertel & Bühler (1978). The optical set-up is sketched in figure 8. The differential interferometer consists of two Wollaston prisms W_1 and W_2, two objectives O_1 and O_2, the two polarizers P_1 and P_2, the $\lambda/2$ plate and the camera objective O giving an image of the test section on the film K. The light source Q is a high-pressure Hg lamp with a monochromatic filter. The interferometer is set on infinite fringe spacing. The components of density differences in direction of the interferometric beam separation are visualized. The differential interferometer can be made sensitive to horizontal or vertical density gradients by simply rotating the prisms around the axis of the objectives.

Differential interferograms for the non-rotating case are shown in figure 10. The test fluid is silicone oil. In figure 10(*a*) the interferometer is adjusted with vertical beam separation so that lines of constant vertical density differences can be seen. Lines of constant horizontal density differences become visible with horizontal beam separation as shown in figure 10(*b*). The heat conduction state in the vertical direction has been eliminated and the interference fringes look very like the streamlines. Figure 10(*c*) shows the principal sketch of the convection rolls.

3.4. *Results in silicone oil*

Silicone oil is a very viscous medium. In the investigated region of the speed of rotation the Taylor numbers were of order of $Ta = 10^3$. The tests were carried out so that for a constant Taylor number the Rayleigh number was quasi-statically increased. In

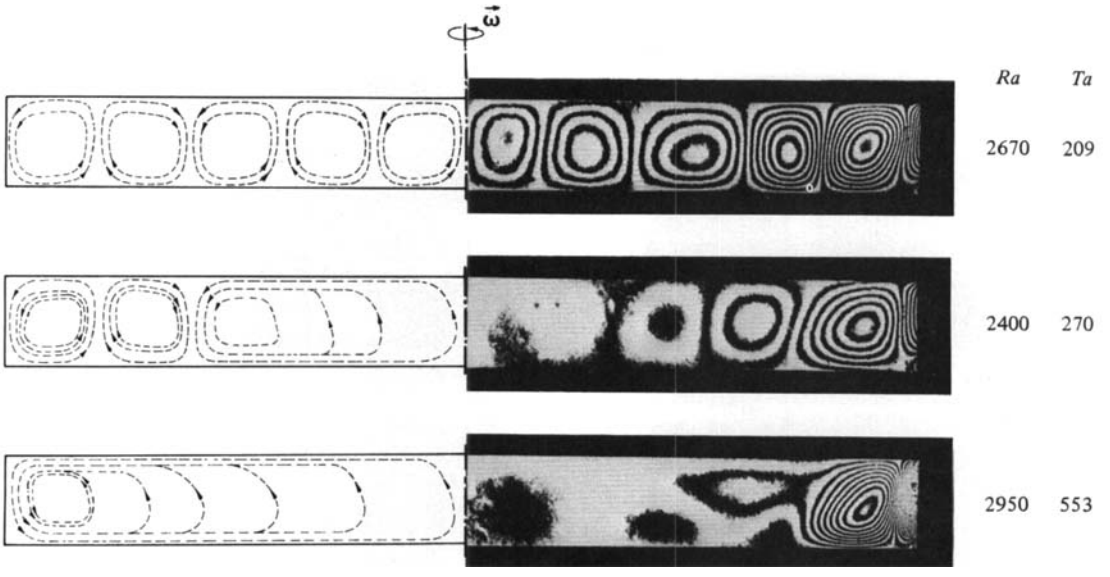

FIGURE 11. Influence of the rotation on the flow configuration in test fluid silicone oil, (x, z)-plane.

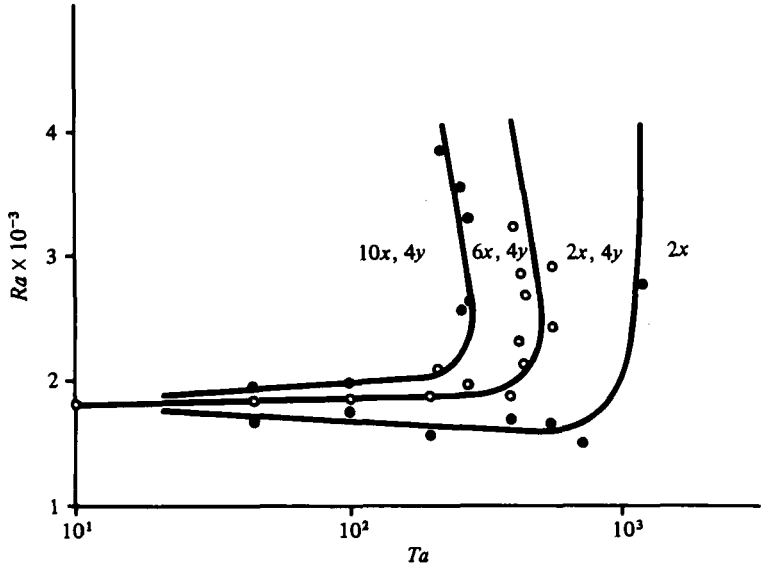

FIGURE 12. Stability regions of the different flow configurations, test fluid silicone oil.

figure 11 the flow configurations are shown symmetric to the rotation axis. On the left are shown the principal sketches of the flow and on the right the corresponding interferograms. Lines of equal horizontal density differences are visible. Three different flow configurations, which are essentially the result of the centrifugal force, can be recognized.

For small Taylor numbers ten convection rolls were measured. The amplitude of the

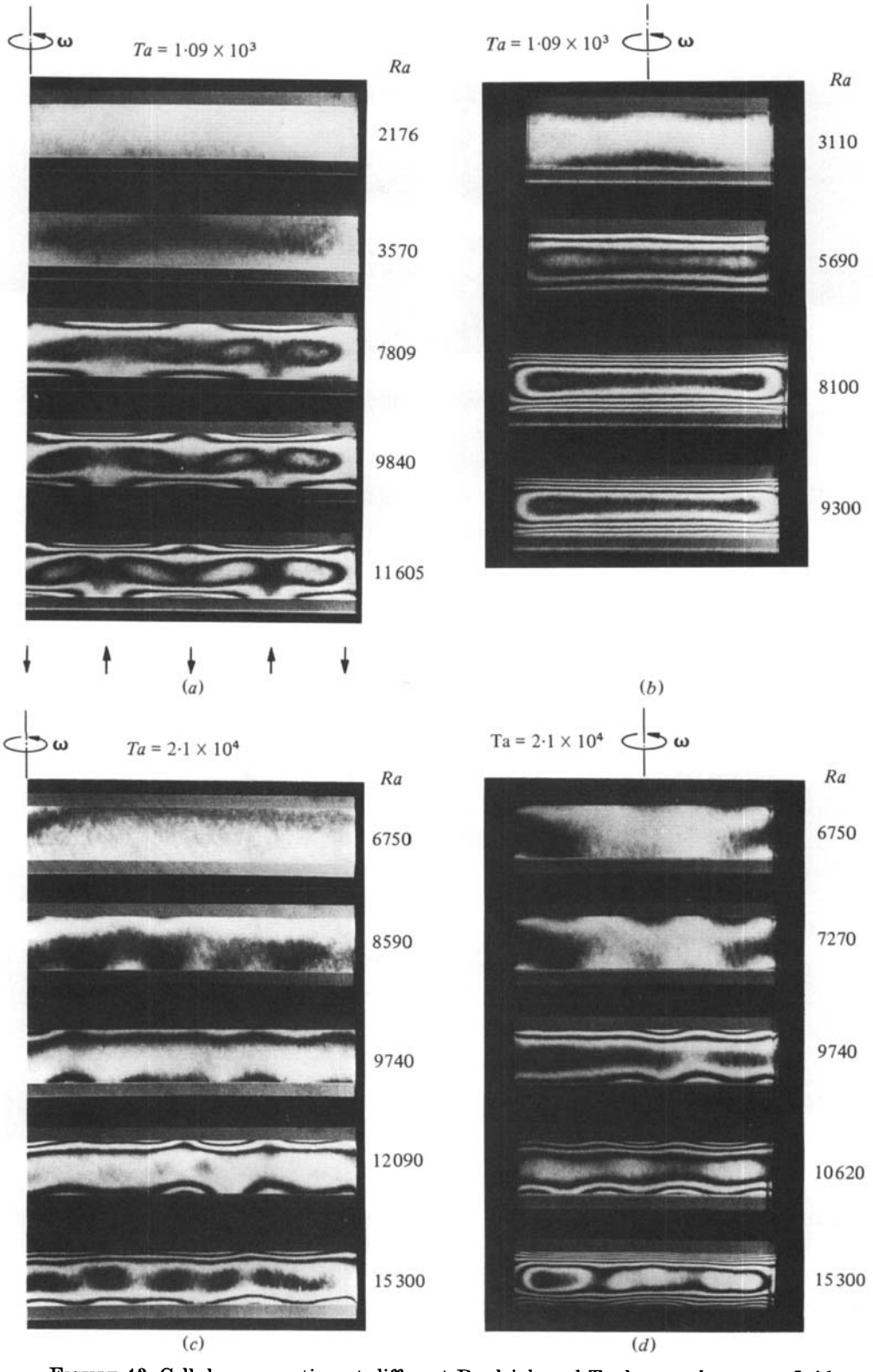

FIGURE 13. Cellular convection at different Rayleigh and Taylor numbers, test fluid nitrogen. (*a*, *b*) Steady convection; (*c*, *d*) time-dependent convection.

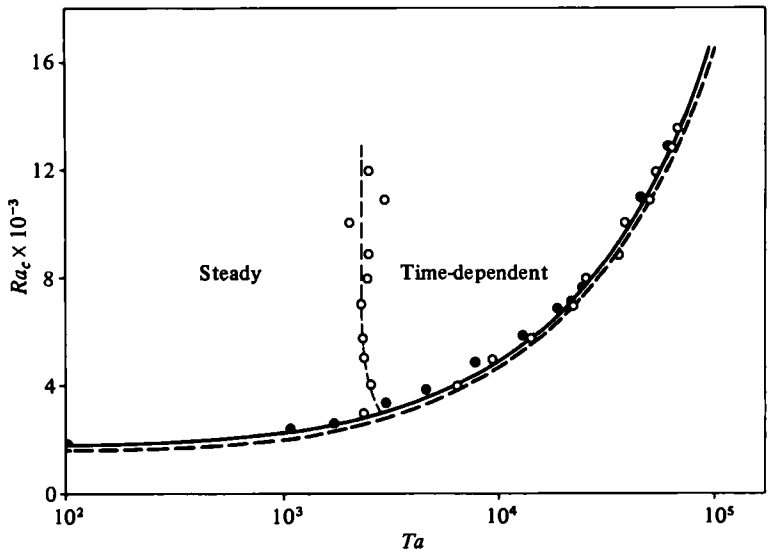

FIGURE 14. Critical Rayleigh number as a function of the Taylor number for nitrogen. ●, Increasing Ra with Ta = constant, Bühler (1979); ○, increasing Ta with Ra = constant, Oertel & Kirchartz (1978); ——, linear theory, box $H_x = 10$, $H_y = 4$, Bühler (1979); – – –, analytical result, infinite layer, Chandrasekhar (1961).

flow grows from the rotation axis to the side boundary through the influence of centrifugal force, but the buoyancy effect dominates. With increasing Taylor number the centrifugal force increases so that the flow pattern becomes more spacious. At a Taylor number $Ta = 270$, six convection rolls have been observed. At $Ta = 553$, only the centrifugally driven basic flow can be seen. The x-rolls in the (x, z)-plane are slightly modulated by a periodic motion of y-rolls in the (y, z)-plane.

In the stability diagram in figure 12 the different flow regions are defined. For $Ta = 0$ the critical Rayleigh number without rotation was measured. The destabilizing effect of the centrifugal force is the same as described by Homsy & Hudson (1971*b*).

These effects cannot be described in the physical model which underlies the linear stability theory of this work, because it neglects centrifugal force. The validity region is already exceeded for silicone oil for small Taylor numbers, as can be seen in figure 11.

3.5. *Results in nitrogen*

When the test fluid is nitrogen, the influence of the Coriolis force dominates that of the centrifugal force because the relative velocity in gases is greater by a factor of 10^2. In figure 13 the development of convection in nitrogen for two different Taylor numbers is illustrated by an interferogram series with lines of constant vertical density differences. Here, the optical path differences are significantly smaller than those in silicone oil. Only a few fringes can be visualized in nitrogen.

In figures 13 (*a*, *b*) the convection rolls in the (x, z)-plane can be seen from the rotation axis in the middle of the box to the side wall. Figures 13 (*b*), (*d*) show the convection rolls in the (y, z)-plane, i.e. the view along the long side of the box. Figures 13 (*a*), (*b*) show the development of cellular convection at a Taylor number $Ta = 1{\cdot}09 \times 10^3$ ($\simeq$ 10 rev./min). The basic state of heat conduction is superimposed by cellular

convection. Because of the small centrifugal force, the flow is symmetrical to the rotation axis in the middle of the box. Eight x-rolls are formed, whose amplitudes increase with increasing Rayleigh number. The regions of the flow pattern can be recognized from the periodic interference fringes. In an area of upward motion there are many fringes at the upper horizontal plate while, in an area of downward motion, they are at the lower horizontal plate. In figure 12(*b*), viewed from along the longer side of the rectangular box, a modulation along the axis of the convection roll can be observed.

This process also appears in the non-rotating container as is shown in the papers of Oertel (1980) and Bühler, Kirchartz & Oertel (1979). In the critical state there always exists a modulation along the axis of the dominant convection rolls. At supercritical Rayleigh numbers steady x-rolls are dominant. In figures 13(*c*), (*d*), the experiments at the Taylor number $Ta = 2{\cdot}1 \times 10^4$ ($\simeq 50$ rev./min) can be seen. The cellular convection starts at substantially higher Rayleigh numbers. The flow is three-dimensional and time-dependent. This can be illustrated experimentally by the periodic wavy interference fringes in the (x, z)- and (y, z)-planes.

Time-dependent convection in rotating containers appears at Taylor numbers $Ta > 1{\cdot}5 \times 10^3$, with $H_x = 10$, $H_y = 4$ in the box investigated. This results from the non-existence of steady solutions in rotating fluid layers above a certain Taylor number.

The physical model described in § 2.1 is very well satisfied when nitrogen is the test medium. Figure 14 shows the comparison of the theoretical and experimental results. The critical Rayleigh number is plotted as a function of the Taylor number. The solid curves give the result of the linear stability theory for the box. The dashed lines indicate the results of Chandrasekhar (1961) for infinite horizontal fluid layers. Together with the experimental results obtained by increasing the Rayleigh number and holding the Taylor number constant, are shown the results of Oertel (1978) and Oertel & Kirchartz (1979) for which the Taylor number was increased with the Rayleigh number held constant. The values of the critical Rayleigh numbers are independent of the way in which the experiments are carried out. Within the scope of the experimental accuracy the agreement between theory and experiments is very good. The Coriolis force has a significantly stabilizing effect. The values of measured and evaluated critical Rayleigh numbers agree also in the time-dependent region. The observation of this time-dependent convection flow is not identical with Chandrasekhar's (1961) oscillatory modes at low Prandtl numbers. Rather, it is related to the non-existence of steady, stable finite-amplitude convection above a certain Taylor number.

The stability calculations from Küppers & Lortz (1969) have shown that no stable, steady convective flow exists if the Taylor number exceeds the critical value $Ta = 2285$ for an infinite horizontal fluid layer, infinite Prandtl number and free boundary conditions. These calculations were extended by Küppers (1970) to fixed horizontal boundaries and variable Prandtl numbers. He found that the critical value for Ta decreases with decreasing Prandtl number. For nitrogen as the test fluid with $Pr = 0{\cdot}71$, the critical value is about $Ta \simeq 600$. The value observed experimentally in the rectangular box of $H_x = 10$, $H_y = 4$ is $Ta \simeq 1500$. The difference can be explained by the effect of side walls, which have a stabilizing effect on the onset of a time-dependent flow. Above this Taylor number, and increasing Rayleigh number from a

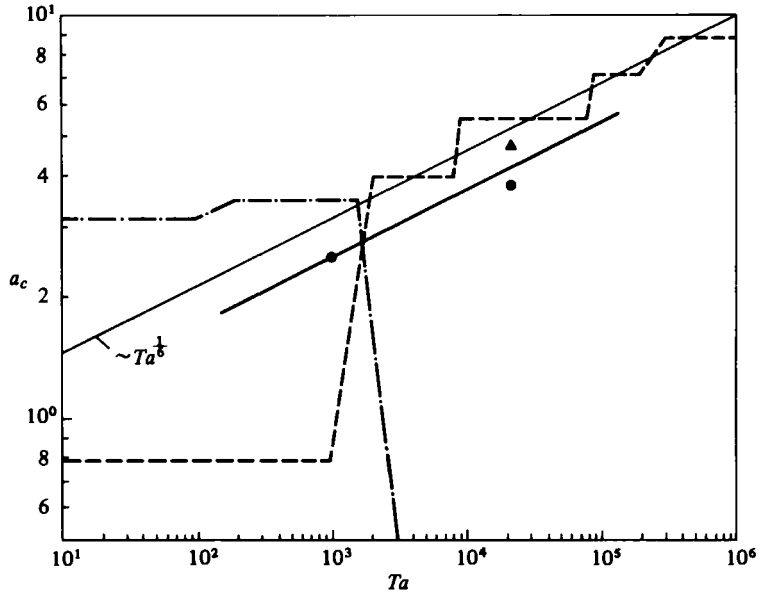

FIGURE 15. Dimensionless wavenumber compared with experiments for nitrogen, box $H_x = 10$, $H_y = 4$. The symbols represent experimental data, the lines the theory. ●, – · – · –, x-rolls; ▲, – – – –, y-rolls.

subcritical value, there is a transition from pure conduction to a time-dependent convective flow.

Special features of the time-dependent behaviour of a convective flow in rotating systems with respect to the calculations of Clever & Busse (1979) were investigated by Busse & Heikes (1980). The influence of the side boundaries in their extended fluid layer is less significant than in our rectangular box and therefore a direct comparison of the Taylor number above their time-dependent convection flow is not possible.

Figure 15 shows the theoretical and experimental dimensionless wavenumbers as functions of the Taylor number. Convection rolls which are oriented along the shorter side of the rectangular box are dominated for $Ta < 1{\cdot}5 \times 10^3$ in the box with $H_x = 10$ and $H_y = 4$. The rolls orient themselves along the longer side at Taylor numbers larger than $1{\cdot}5 \times 10^3$. The theoretical results are plotted in figure 14 as the broken and dotted lines. The step functions result from the discrete number of rolls in the convection box. The number of convection rolls increases with increasing Taylor number. This effect can also be seen in the interferograms of figure 13 in the steady and time-dependent convection. The dimensionless wavenumbers for these experiments have been plotted in figure 15. The asymptotic behaviour $a_c \sim Ta^{\frac{1}{5}}$ of the theory is very well confirmed for an average wavelength in the (x,z)- and (y,z)-planes at the Taylor number $Ta = 2{\cdot}1 \times 10^4$.

	Bühler (1979)	Niiler & Bisshop (1965)	Chandrasekhar (1961)
Geometry	Box $H_x = 10$, $H_y = 4$	Fixed horizontal boundaries, infinite layer	Free horizontal boundaries, infinite layer
Taylor number	10^5	10^6	$\to \infty$
c_1	8·0	7·11	8·69
c_2	1·1 theory 0·8 experiment	—	1·30

TABLE 3. Constants compared with that of the asymptotic solutions.

4. Comparison with asymptotic solution

Asymptotic solutions are known for steady convective flows and large Taylor numbers from the analytical theory of Chandrasekhar (1961), with the following results:

$$Ra_c \to c_1 Ta^{\frac{2}{3}}, \quad a_c \to c_2 Ta^{\frac{1}{3}}.$$

The powers are determined by the differential equation of the eigenvalue problem. For infinite fluid layers with free horizontal boundaries the values are $c_1 = 8{\cdot}69$ and $c_2 = 1{\cdot}30$. Niiler & Bishop (1965) calculated the $c_1 = 7{\cdot}11$ for fixed horizontal boundaries and for the intermediate Taylor number, $Ta = 10^6$. Homsy & Hudson (1971*a*) shows that the asymptotic constants c_1 and c_2 do not depend on the boundary conditions or aspect ratio except when H_x, $H_y \ll 1$. Our theoretical and experimental results for rotating rectangular boxes with H_x, $H_y > 1$ confirm the asymptotic power laws. The constants c_1 and c_2 determined from the theory and experiments are restricted to intermediate Taylor numbers of $Ta \simeq 10^5$. We find $c_1 = 8{\cdot}0$ for the stability behaviour from theory and experiments. The behaviour of the wavenumbers $c_2 = 1{\cdot}1$ is obtained from the theory and $c_1 = 0{\cdot}8$ from the experiments. The difference could possibly arise as a result of the influence of the small centrifugal effects in the experiments. These results are summarized together with previously published results in table 3. We find that the constants c_1 and c_2 for intermediate Taylor numbers are smaller than the correct asymptotic values predicted for Taylor numbers $Ta \to \infty$.

5. Conclusion

The optical measuring technique has been successfully used for the direct observation of the critical Rayleigh number and for the visualization and quantitative determination of the density field of the convection flow. The flow configuration in the form of cellular structure changes its orientation when the Taylor number is above a certain critical value. The wavelength decreases as the Taylor number increases.

In our experiments, two test fluids are used: one is silicone oil which has a high Prandtl number and the other is nitrogen, which has a low Prandtl number. It has been found that the centrifugal force dominates in the case of fluid of high Prandtl number, e.g. silicone oil, and that the Coriolis force is dominant in the case of fluid with low Prandtl number.

In our physical model, a linear stability theory with Boussinesq's approximation, the centrifugal force is neglected. Therefore, our theoretical model is applicable only to the convective flow of fluid with low Prandtl number. Our experimental results confirm this fact. Our experimental results of nitrogen agree closely with theoretical calculations for the stability behaviour and flow configuration in the region of stationary convective flow when $Ta < 1500$. When $Ta > 1500$, the convective flow is unsteady. We cannot predict the unsteady convective flow by our theoretical model. However, the theoretical results for the onset of convection can also be applied successfully to time-dependent convective flow. Further theoretical investigation of the time-dependent convective flow is needed.

The authors wish to express their appreciation to Professor Dr-Ing. J. Zierep for valuable suggestions and stimulating discussions during the investigations. All numerical calculations have been done with the UNIVAC 1108 of the computer centre of the University of Karlsruhe.

Appendix. Trial functions

For the velocity field we used the functions as they were described by Harris & Reid (1958):

$$C_{pj}(x) = \frac{\cosh(\lambda_{pj}x)}{\cosh(\frac{1}{2}\lambda_{pj})} - \frac{\cos(\lambda_{pj}x)}{\cos(\frac{1}{2}\lambda_{pj})}, \tag{A 1}$$

$$S_{pj}(x) = \frac{\sinh(\mu_{pj}x)}{\sinh(\frac{1}{2}\mu_{pj})} - \frac{\sin(\mu_{pj}x)}{\sin(\frac{1}{2}\mu_{pj})}; \tag{A 2}$$

$C_{pj}(x)$ is an even function and $S_{pj}(x)$ is an odd function, both of which are equal to zero for $x = \pm\frac{1}{2}$. The arguments λ_{pj} and μ_{pj} were so chosen that the derivatives of the functions are also zero for $x = \pm\frac{1}{2}$. For the temperature field the simple trigonometrical function is sufficient. The Coriolis term always requires an odd function, while the convection motion without rotation can be described with both even and odd functions, depending on whether an even or odd number of rolls appears.

Function system I

With an odd number of rolls in the (x, z)- and (y, z)-planes,

$$\psi_j = C_{pj}\left(\frac{x}{H_x}\right)\cos\left((2q_j-1)\frac{\pi y}{H_y}\right)C_{rj}(z), \tag{A 3}$$

$$\phi_j = \cos\left((2p_j-1)\frac{\pi x}{H_x}\right)C_{qj}\left(\frac{y}{H_y}\right)C_{rj}(z), \tag{A 4}$$

$$T^*_{1j} = \sin\left(2p_j\frac{\pi x}{H_x}\right)\cos\left((2q_j-1)\frac{\pi y}{H_y}\right)\cos((2r_j-1)\pi z), \tag{A 5}$$

$$T^*_{2j} = -\cos\left((2p_j-1)\frac{\pi x}{H_x}\right)\sin\left(2q_j\frac{\pi y}{H_y}\right)\cos((2r_j-1)\pi z). \tag{A 6}$$

Function system II

With an even number of rolls in the (x, z)-plane and odd number in the (y, z)-plane

$$\psi_j = S_{pj}\left(\frac{x}{H_x}\right)\cos\left((2q_j-1)\frac{\pi y}{H_y}\right)C_{rj}(z), \tag{A 7}$$

$$\phi_j = \sin\left(2p_j\frac{\pi x}{H_x}\right)C_{qj}\left(\frac{y}{H_y}\right)C_{rj}(z), \tag{A 8}$$

$$T^*_{1j} = \cos\left((2p_j-1)\frac{\pi x}{H_x}\right)\cos\left((2q_j-1)\frac{\pi y}{H_y}\right)\cos\left((2r_j-1)\pi z\right), \tag{A 9}$$

$$T^*_{2j} = -\sin\left(2p_j\frac{\pi x}{H_x}\right)\sin\left(2q_j\frac{\pi y}{H_y}\right)\cos\left((2r_j-1)\pi z\right). \tag{A 10}$$

By exchanging the co-ordinates x and y an odd number of rolls can be also described in the (x, z)-plane with this function system and an even number of rolls in the (y, z)-plane.

With these trial functions the integrals of the Galerkin equations (2.9)–(2.10) can be calculated according to the following relations, whereby the integrals comply with the elements of the matrices **A**, **B**, **C** and **D**.

$$\begin{aligned}\mathbf{A} = a_{kj} &= \int_V \mathbf{v}_k\,\Delta\mathbf{v}_j\,dV - Ta^{\frac{1}{2}}\int_V(\mathbf{e}_z\times\mathbf{v}_j)\,\mathbf{v}_k\,dV\\ &= \int_V(u_k\,\Delta u_j + v_k\,\Delta v_j + w_{1k}\,\Delta w_{1j} + w_{2k}\,\Delta w_{2j})\,dV - Ta^{\frac{1}{2}}\int_V(u_j v_k - v_j u_k)\,dV,\end{aligned} \tag{A 11}$$

$$\mathbf{B} = b_{kj} = \int_V w_k T^*_j\,dV = \int_V(w_{1k}T^*_{1j} + w_{2k}T^*_{2j})\,dV, \tag{A 12}$$

$$\mathbf{C} = c_{kj} = \int_V w_j T^*_k\,dV = \int_V(w_{1j}T^*_{1k} + w_{2j}T^*_{2k})\,dV, \tag{A 13}$$

$$\mathbf{D} = d_{kj} = \int_V T^*_k\,\Delta T^*_j\,dV = \int_V(T^*_{1k}\,\Delta T^*_{1j} + T^*_{2k}\,\Delta T^*_{2j})\,dV. \tag{A 14}$$

The eigenvalue problem resulting from the Galerkin equations is solved numerically using the Hessenberg method and the computer program of Smith *et al.* (1976).

REFERENCES

Abell, S. & Hudson, J. L. 1975 An experimental study of centrifugal driven free convection in a rectangular cavity. *Int. J. Heat Mass Transfer* **18**, 1415–1423.

Bühler, K. 1979 Zellularkonvektion in rotierenden Behältern. Dissertation Karlsruhe, Fortschritt-Berichte VDI-Z., Reihe 7, Nr. 54.

Bühler, K., Kirchartz, K. R. & Oertel, H. 1979 Steady convection in a horizontal fluid layer. *Acta Mech.* **31**, 155–171.

Busse, F. H. & Heikes, K. E. 1980 Convection in a rotating layer: a simple case of turbulence. *Science* **208**, 173–175.

Catton, I. 1970 Convection in a closed rectangular region: the onset of motion. *J. Heat Transfer* **92**, 186–188.

Chandrasekhar, R. S. 1961 *Hydrodynamic and Hydromagnetic Stability*. Oxford University Press.

CLEVER, R. M. & BUSSE, F. H. 1979 Nonlinear properties of convection rolls in a horizontal layer rotating about a vertical axis. *J. Fluid Mech.* **94**, 609–627.

DAVIS, S. H. 1967 Convection in a box: linear theory. *J. Fluid Mech.* **30**, 465–478.

DAVIES-JONES, R. P. & GILMAN, P. A. 1971 Convection in a rotating annulus uniformly heated from below. *J. Fluid Mech.* **46**, 65–81.

FINLAYSON, B. A. 1968 The Galerkin method applied to convective instability problems. *J. Fluid Mech.* **33**, 201–208.

FRICK, H. & CLEVER, R. M. 1980 Einfluß der Seitenwände auf das Einsetzen der Konvektion in einer horizontalen Flüssigkeitsschicht. *Z. angew. Math. Phys.* **31**, 502–513.

GERSHUNI, G. Z. & ZUKHOVITSKII, E. M. 1976 *Convective Instability of Incompressible Fluids.* Jerusalem: Keter.

GILMAN, P. A. 1973 Convection in a rotating annulus uniformly heated from below. Part 2. Nonlinear results. *J. Fluid Mech.* **57**, 381–400.

GRAY, D. D. & GIORGINI, A. 1976 The validity of the Boussinesq approximation. *Int. J. Heat Mass Transfer* **19**, 545–551.

GREENSPAN, H. P. 1968 *The Theory of Rotating Fluids.* Cambridge University Press.

HARRIS, D. L. & REID, W. H. 1958 On orthogonal functions which satisfy four boundary conditions. *Astrophys. J. Suppl.* Series 3, 429–453.

HOMSY, G. M. & HUDSON, J. L. 1971*a* The asymptotic stability of a bounded rotating fluid heated from below: conductive basic state. *J. Fluid Mech.* **45**, 353–373.

HOMSY, G. M. & HUDSON, J. L. 1971*b* Centrifugal convection and its effect on the asymptotic stability of a bounded rotating fluid heated from below. *J. Fluid Mech.* **48**, 605–624.

HOMSY, G. M. & HUDSON, J. L. 1972 Stability of a radially bounded rotating fluid heated from below. *Appl. Sci. Res.* **26**, 33–66.

HOPFINGER, E. J., ATTEN, P. & BUSSE, F. H. 1979 Instability and convection in fluid layers: A report on Euromech 106. *J. Fluid Mech.* **92**, 217–240.

HUDSON, J. L. 1979 Experiments on centrifugally driven, thermal convection in a rotating cylinder. *J. Fluid Mech.* **86**, 147–159.

HUNTER, C. & RIAHI, N. 1975 Nonlinear convection in a rotating fluid. *J. Fluid Mech.* **72**, 433–454.

KOSCHMIEDER, E. L. 1967 On convection on a uniformly heated rotating plane. *Beitr. z. Phys. Atmos.* **40**, 216–225.

KÜPPERS, G. 1970 The stability of steady finite amplitude convection in a rotating fluid layer. *Phys. Letters* A, **32**, 7–8.

KÜPPERS, G. & LORTZ, D. 1969 Transition from laminar convection to thermal turbulence in a rotating fluid layer. *J. Fluid Mech.* **35**, 609–620.

NIILER, P. P. & BISSHOP, F. E. 1965 On the influence of Coriolis force on onset of thermal convection. *J. Fluid Mech.* **22**, 753–761.

OERTEL, H. 1978 Einfluß der Rotation auf die stationäre Zellularkonvektion. *Z. angew. Math. Mech.* **59**, 248–252.

OERTEL, H. 1979 Thermische Zellularkonvektion. Habilitationsschrift Universität Karlsruhe (TH).

OERTEL, H. 1980 Three-dimensional convection within rectangular boxes. *The 19th National Heat Transfer Conf., Orlando, Florida, HTD*, vol. 8.

OERTEL, H. 1981 *J. Fluid Mech.* (submitted).

OERTEL, H. & BÜHLER, K. 1978 A special differential interferometer used for heat convection investigations. *Int. J. Heat Mass Transfer* **21**, 1111–1115.

OERTEL, H., BÜHLER, K., KIRCHARTZ, K. R. & SRULIJES, J. 1978 Experimentelle und theoretische Untersuchung der Zellularkonvektion. *Mitteilungen des Instituts für Strömungslehre und Strömungsmaschinen, Universität (TH) Karlsruhe* Nr. 24, pp. 40–72.

OERTEL, H. & KIRCHARTZ, K. R. 1979 Influence on initial and boundary conditions on Bénard convection. *Recent Developments in Theoretical and Experimental Fluid Mechanics.* Springer.

OSTRACH, S. 1972 Natural convection in enclosures. *Adv. Heat Transfer* **8**, 161–227.

ROSSBY, H. T. 1969 A study of Bénard convection with and without rotation. *J. Fluid Mech.* **36**, 309–335.

SMITH, B. T., BOYLE, J. M., DONGARRA, J. J., GARBOW, B. S., IKEBE, Y., KLEMA, V. C. & MOLER, C. B. 1976 *Matrix Eigensystem Routines – EISPACK Guide*, Lecture Notes in Computer Science, vol. 6. Springer.

SOMMERVILLE, R. C. & LIPPS, F. B. 1973 A numerical study in three space dimensions of Bénard convection in a rotating fluid. *J. Atmospheric Sci.* **30**, 590–596.

STORK, K. & MÜLLER, U. 1972 Convection in boxes: experiments. *J. Fluid Mech.* **54**, 599–611.

SPIEGEL, E. A. & VERONIS, G. 1960 On the Boussinesq approximation for a compressible fluid. *Astrophys. J.* **131**, 442–447.

TORREST, M. A. & HUDSON, L. 1974 The effect of centrifugal convection on the stability of a rotating fluid heated from below. *Appl. Sci. Res.* **29**, 273–289.

VERONIS, G. 1968 Large-amplitude Bénard convection in a rotating fluid. *J. Fluid Mech.* **31**, 113–139.